Research Article Vol. 29, No. 4 / 15 February 2021 / Optics Express 5635
Optics EXPRESS

Invariance of the r^2-ln(F) relationship and attainable precision in ultrafast laser ablation experiments

BOYANG ZHOU,[1] ARAVINDA KAR,[1,2] M. J. SOILEAU,[1,2,3,4] AND XIAOMING YU[1,2,*]

[1] *CREOL, The College of Optics and Photonics, University of Central Florida, Orlando, Florida 32816, USA*
[2] *Townes Laser Institute, The College of Optics and Photonics, University of Central Florida, Orlando, Florida 32816, USA*
[3] *Department of Physics, University of Central Florida, Orlando, Florida 32816, USA*
[4] *Department of Electrical and Computer Engineering, University of Central Florida, Orlando, Florida 32816, USA*
[*] *yux@creol.ucf.edu*

Abstract: Pursuing ever-smaller feature size in laser-based lithography is a research topic of vital importance to keep this technique competitive with other micro-/nano-fabrication methods. Features smaller than the diffraction-limited spot size can be obtained by "thresholding", which utilizes the deterministic nature of damage threshold with ultrashort laser pulses and is achieved by precisely tuning pulse energies so that only the central portion of the focal spot produces permanent modification. In this paper, we examine the formulation commonly used to describe thresholding and show that the relationship between feature size (r) and laser fluence (F) is invariant with respect to the nature of laser absorption. Verified by our experiments performed on metal, semiconductor, and dielectric samples, such invariance is used to predict the smallest feature size that can be achieved for different materials in a real-world system.

© 2021 Optical Society of America under the terms of the OSA Open Access Publishing Agreement

1. Introduction

The deterministic nature of ultrafast laser-induced material modification paves the way for high-precision processing of a wide range of materials with feature sizes similar to Gaussian focal spots, which are limited by light diffraction [1–10]. Techniques to reduce feature size below the diffraction limit include nano-grating [11], stimulated emission depletion (STED) [12], partially overlapping focal spots [13], and many other methods [14–16]. The most straightforward way is so-called "thresholding", by which the pulse energy is controlled so precisely that only a portion of the focal fluence distribution exceeds the threshold for permanent modification [17]. Thresholding, in conjunction with nonlinear (multiphoton) absorption in wide-bandgap materials, is often invoked as the reason for feature size below the diffraction-limited spot size.

In principle, thresholding itself is capable of achieving a very small feature size according to the formula derived from a Gaussian profile for materials with deterministic thresholds [18]. Thus the question is how different absorption mechanisms (linear or nonlinear) affect thresholding and as a result the relationship between feature size and pulse energy. This topic has been explored by Fischer *et al*. in the context of multiphoton polymerization [19], and M. Gedvilas *et al*. explored multiphoton absorption enhancement by dual-wavelength double-pulse laser irradiation [20]. Recently, Garcia-Lechuga *et al*. have shown that such relationship is invariant for dielectrics with different bandgaps [21]. In this paper, we will theoretically and experimentally show that such invariance is consistent with the well-known single-photon model and provides the ability to predict the smallest feature size in experiments.

#418288 https://doi.org/10.1364/OE.418288
Journal © 2021 Received 23 Dec 2020; revised 29 Jan 2021; accepted 1 Feb 2021; published 5 Feb 2021

2. Theory

We start from the model derived by Liu [18], which relates feature size r_{th} with peak laser fluence F_0 as

$$2r_{\mathrm{th}}^2 = w_0^2 \cdot \ln\frac{F_0}{F_{\mathrm{th}}}, \tag{1}$$

where w_0 is the $1/e^2$ radius of the Gaussian focus, and F_{th} is the threshold fluence at which features start to form on the surface. Originally developed for determining the size of laser focal spot w_0, Eq. (1) has been commonly used to determine the damage threshold F_{th} for various types of materials such as semiconductors and metals [22–24], which predominantly absorb laser energy through single-photon processes. This is due to the presence of a large amount of initial free electrons [9,25].

However, the mechanism of laser ablation in dielectrics is different since the density of initial free electrons is small, and feature generation is related to the accumulation of free electrons through multiphoton ionization (MPI) and avalanche ionization (AI) processes. Here, we consider a feature forms when the density of free electrons is equal to or higher than the critical density, which is in accordance with the previous results [4–7]. It is worth pointing out that the total laser energy coupled to the electron subsystem is also reported as the laser breakdown threshold when high-intensity few-cycle laser pulses are applied [26]. To understand the relationship between feature size and laser intensity in dielectrics, the following derivation is conducted for two cases depending on which process is dominant. When MPI is dominant, a rate equation can be written as

$$\frac{\partial n_e(r,t)}{\partial t} = \sigma I^k(r,t), \tag{2}$$

$$I(r,t) = I_0 e^{-\frac{2r^2}{w_0^2}} e^{-4\ln(2)\frac{t^2}{\tau^2}}. \tag{3}$$

Here, n_e is the density of conduction-band (CB) free electrons excited from the valence band (VB) through MPI, σ is the MPI coefficient [4] and k is the order of MPI; $I(r,t)$ is the laser intensity with peak intensity I_0, FWHM (full-width-at-half-maximum) pulse duration τ, and focal spot size w_0 measured at the $1/e^2$ level. For simplicity, in Eq. (2), recombination of electron-hole pairs is ignored. This is justified because we are interested in the events leading to the maximum n_e at which features are formed [4]. We also exclude free-carrier diffusion because the diffusion length is estimated to be small (<100 nm) compared to w_0 used in this experiment [27,28]. This exclusion of free-carrier diffusion needs to be examined when features much smaller than the laser wavelength are desired. The total density of CB free electrons $n_e(r,t{=}\infty)$ can be solved by integration over time as

$$n_e(r,t=\infty) = n_0 + \sigma \int_{-\infty}^{\infty} e^{-k\cdot 4\ln 2\frac{t'^2}{\tau^2}} dt' I_0^k e^{-k\frac{2r^2}{w_0^2}}, \tag{4}$$

where n_0 is the initial density of free electrons $n_e(r,t{=}{-}\infty)$. Since almost all the CB free electrons are generated through MPI in semiconductors and metals, n_0 can be seen as zero when $t = -\infty$. The integral in Eq. (4) is a Gaussian integral which can be solved directly. Features start to form when n_e reaches the critical density n_{th}. This is equivalent to setting $r = r_{\mathrm{th}}$ in the last exponential term in Eq. (4), and we arrive at

$$n_{\mathrm{th}} = n_e(r = r_{th}, t = \infty) = \sigma\sqrt{\frac{\pi}{k\cdot 4ln2}}\tau I_0^k e^{-k\frac{2r_{\mathrm{th}}^2}{w_0^2}}, \tag{5}$$

Taking the natural logarithm on both sides, we have

$$2r_{\mathrm{th}}^2 = w_0^2 \ln(I_0) + \ln\left(\frac{\sigma\tau\sqrt{\pi}}{\sqrt{k}\cdot 2\sqrt{\ln 2}\cdot n_{\mathrm{th}}}\right)\frac{w_0^2}{k}. \tag{6}$$

Note that mathematically the argument of the ln() function should be dimensionless. Writing Eq. (6) in the current form requires adding factors such as 1 W/cm^2 which are omitted for simplicity. Such factors are only for a mathematical reason and ignoring it will not affect the relationship between r_{th} and F_0. Since the relationship between peak intensity I_0 and peak fluence F_0 follows $I_0 = \frac{2F_0}{\tau} \cdot \sqrt{\frac{ln2}{\pi}}$, Eq. (6) can be rewritten in terms of F_0 as

$$2r_{\text{th}}^2 = w_0^2 \ln(F_0) + \ln\left(\frac{\sigma\left(2\sqrt{ln2}\right)^{k-1}}{\left(\tau\sqrt{\pi}\right)^{k-1}\sqrt{k}\cdot n_{\text{th}}}\right)\frac{w_0^2}{k}, \tag{7}$$

The last term in Eq. (7) is independent of F_0, so we can rename it as C_{MPI}, and Eq. (7) can be simplified as

$$2r_{\text{th}}^2 = w_0^2 \ln(F_0) + C_{MPI}. \tag{8}$$

We can see from Eq. (8) that the nonlinearity factor k vanishes from the first term which dictates how feature size r_{th} changes as peak fluence F_0 is varied, resulting in a relationship similar to Eq. (1).

Following a similar procedure, the relationship between r_{th} and F_0 for the AI-dominated case can be derived from the following rate equation

$$\frac{\partial n_e(r,t)}{\partial t} = \eta I(r,t) n_e(r,t), \tag{9}$$

where η is the avalanche coefficient. Different from the MPI-dominated case, n_e is increasing exponentially with respect to t and at the same time, has a spatial distribution due to the Gaussian beam profile, giving rise to a double-exponent as

$$n_e(r, t=\infty) = n_0 e^{\eta \int_{-\infty}^{\infty} e^{-4\ln 2\frac{t'^2}{\tau^2}} dt' I_0 e^{-\frac{2r^2}{w_0^2}}}. \tag{10}$$

Again, using the Gaussian integral and setting $n_{\text{e}}(r=r_{\text{th}},t=\infty)=n_{\text{th}}$ and $r=r_{\text{th}}$, we get

$$n_{\text{th}} = n_0 e^{\eta\sqrt{\frac{\pi}{4ln2}}\tau I_0 e^{-\frac{2r_{\text{th}}^2}{w_0^2}}}. \tag{11}$$

n_0 can be considered as charge carrier density in semiconductors or "seed electrons" provided by MPI (discussed below). By taking the natural logarithm and substituting I_0 with F_0, we obtain

$$2r_{\text{th}}^2 = w_0^2 \ln(F_0) + \ln\left(\frac{\eta}{\ln\left(\frac{n_{\text{th}}}{n_0}\right)}\right) w_0^2. \tag{12}$$

Since all the parameters in the last term are constants, we can rename it as C_{AI}, and Eq. (12) can be simplified as

$$2r_{\text{th}}^2 = w_0^2 \ln(F_0) + C_{AI}. \tag{13}$$

Once again, we arrive at a relationship similar to what Eq. (1) predicts for the change of feature size as a function of laser fluence. It is worth mentioning that although the derivations above deal with two limiting cases, the conclusion still applies when both MPI and AI are present. This can be shown by separating the entire carrier-generation process into two stages, in which MPI provides "seed electrons" whose density is further increased by AI. This technique has been used before to simplify the analysis of the temporal component of the rate equation [4]. In this model, the feature is considered to have a direct response to the local laser fluence. This is because the thermal effects associated with femtosecond laser is low [1–3,29] and the diffusion length of free carriers is much smaller than the laser spot size.

Optics EXPRESS

3. Experimental

Experimentally, we perform single-shot laser lithography experiments on three samples, aluminum 6061, monocrystalline Si (100-oriented), and fused silica (FS, Corning 7980). They represent three types of materials - metal, semiconductor and dielectrics, respectively. Figure 1(a) shows the experiment setup. A femtosecond laser (Pharos, Light Conversion) delivers 167 fs (FWHM) pulses at a center wavelength of 1030 nm with polarization in the x-y plane. The beam is first expanded to a diameter of 10 mm by a Galilean telescope (Lenses 1 and 2) with a magnification of two. The expanded beam is focused by Lens 3 (focal length 200 mm). A variable neutral-density (VND) filter is used to control the laser energy. A three-axis stage with a step resolution of 1 μm is used to adjust the position of the samples to ensure the beam is accurately focused on the front surfaces of the samples. A CMOS camera is used to observe the damage morphology *in*

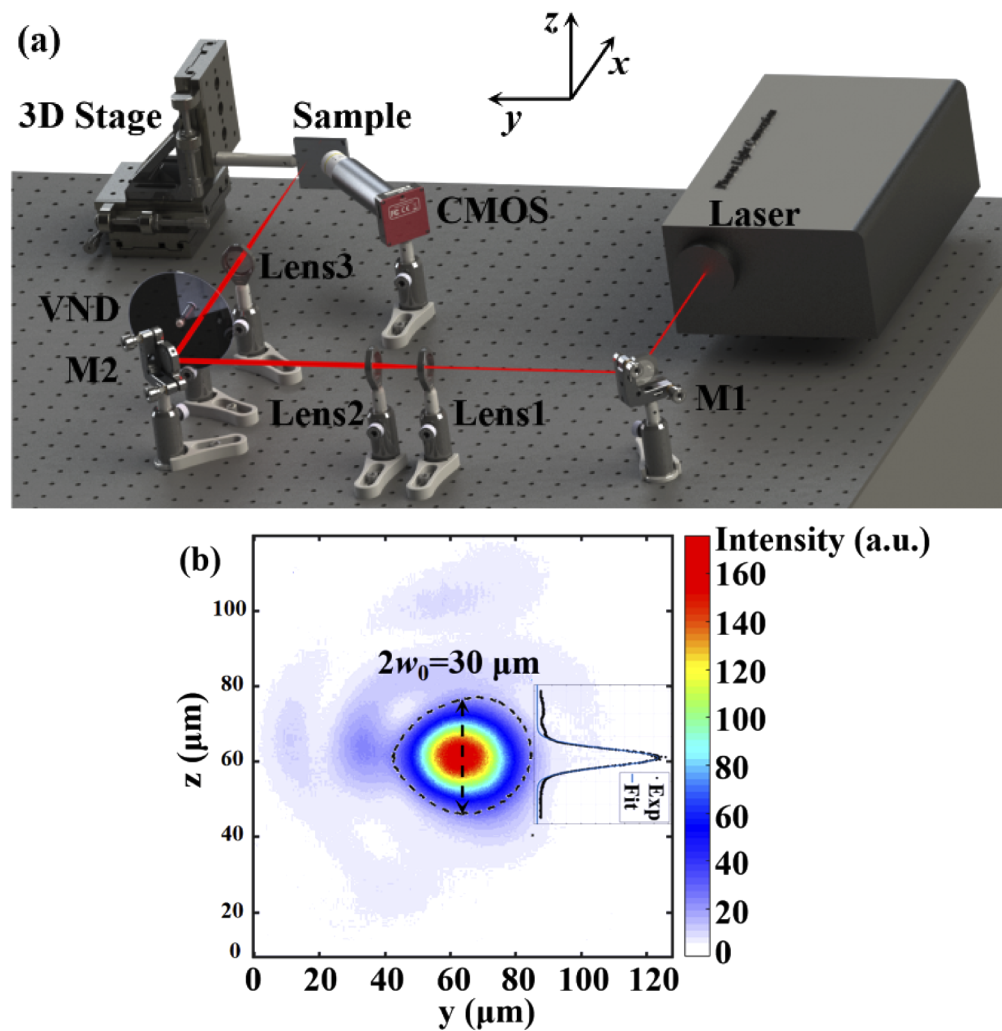

Fig. 1. (a) Experimental setup. M1, M2: mirrors; VND: variable neutral density filter; CMOS: CMOS camera. (b) Profile of the laser focus on the samples. The black dashed line indicates the $1/e^2$ boundary of intensity. The inset shows the Gaussian fitting of experimental data along the vertical direction.

Optics EXPRESS

situ and ensure that the front surfaces of the samples are at the same position. The focal spot on the samples is shown in Fig. 1(b), and the black dashed line marks the $1/e^2$ boundary of the focus. The inset shows a Gaussian fitting of the focus along the vertical direction with a diameter $2w_0 = 30$ µm. Here we choose the fundamental laser wavelength at 1030 nm because it can test the theory in a wide range of optical nonlinearity in bandgap materials.

4. Discussion

Figure 2(a) shows typical morphologies of features created by single pulses. The shapes are nearly circular, similar to the beam profile shown in Fig. 1(b). Features on fused silica have clear boundaries which make it easy to measure feature diameter $2r_{\mathrm{th}}$. For silicon and aluminum, the boundaries are defined as the observable transition between laser modified and pristine surfaces. The feature generated on silicon has a dark spot at the center, which has been attributed to ablation [22]. In our measurement, we use the "modification" size as the feature size $2r_{\mathrm{th}}$ in accordance with that work. For the aluminum sample, the laser ablation experiments were conducted right after polishing so an oxide layer, whose thickness is estimated to be a few nanometers [30,31], is not considered in the model. Thick layers could affect the linear and nonlinear absorption of laser energy, as has been reported before [32]. In all the experiments, the feature diameter $2r_{\mathrm{th}}$ is measured along the vertical direction, which is marked by a black dashed line in Fig. 2(a). Figure 2(b) shows a standard way of extrapolating the damage threshold from the measured $2r_{\mathrm{th}}$ and incident laser fluence F_0 in a semi-log plot [18]. All three data sets have almost the same slope, which is consistent with the theory when the same focal spot size w_0 is used. w_0 is fitted to be 14.6 ± 0.2 µm, which is close to the experimental value. This can be seen more easily in Fig. 2(c), which normalizes F_0 (or I_0) with the corresponding threshold value for each sample. As expected, all data points collapse to a single linear line. It is worth pointing out that the laser ablation threshold would be influenced if multiple pulses are used [33].

An interesting consequence of the invariance relationship between feature size and laser fluence is the predictability of minimum feature sizes achievable for different types of material using one single formula. Replotting the result of Fig. 2(b) to Fig. 3(a) using the linear scale, we can see that feature diameter $2r_{\mathrm{th}}$ changes more quickly above the threshold fluence for material with a smaller threshold. To understand how this affects the smallest feature diameter ($2r_{\mathrm{min}}$) [the lowest data point for each material in Fig. 3(a)], we point out that in our and many others' experiments, a gradual (and discrete) change in laser fluence is used to "approach" ($2r_{\mathrm{min}}$), with a step size ΔF. ΔF should be sufficiently large compared to the pulse-to-pulse fluctuation of a system so that repeatable features can be generated. Our laser has an RMS (root mean square) fluctuation $<0.5\%$.

In Fig. 3(b), we plot the minimum feature sizes, ($2r_{\mathrm{min}}$), achieved in our experiment with values found in the literature (($2r_{\mathrm{min}}$) is normalized with respect to $\sqrt{2}w_0$ reported in those experiments). The curves are obtained from the relationship between feature diameter $2r_{\mathrm{th}}$ and incident fluence F_0 for a material with a certain threshold fluence F_{th}. From Eq. (1), we can derive the relationship between the minimum feature size ($2r_{\mathrm{min}}$) and the threshold fluence F_{th} for a given material with ΔF extracted from the experiments

$$\left((2r_{\mathrm{min}})/\sqrt{2}w_0\right)^2 = \ln((F_{\mathrm{th}} + \Delta F)/F_{\mathrm{th}}). \tag{14}$$

The minimum controllable laser fluence ΔF is 0.08 J/cm^2, which is due to the control resolution of the VND in our system. The minimum feature size ($2r_{\mathrm{min}}$) according to different threshold F_{th} is shown in Fig. 3(b), which is marked as the blue solid line. In addition to our data, data from the work of Liu [18], Korte *et al.* [34], and Garcia-Lechuga *et al.* [21], are included and marked as pink/blue, red, and green. ΔF is read from the plots in those papers and the values are shown in the legend. Solid lines in Fig. 3(b) are fitting results calculated from Eq. (14)

Optics EXPRESS

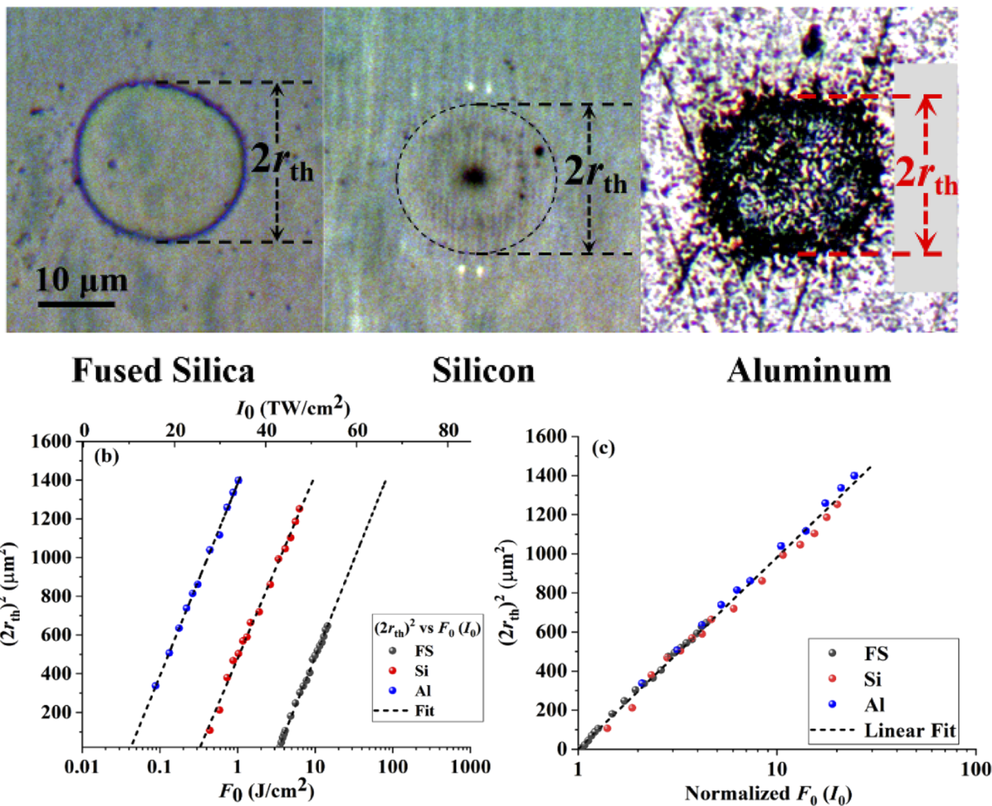

Fig. 2. (a) Optical microscopy images of single-shot laser written features on three different materials (dielectrics, semiconductor, and metal). (b) Relation between square of feature diameter $(2r_{th})^2$ and incident peak fluence F_0 (intensity I_0) plotted in the semi-log scale. (c) relation with F_0 (I_0) normalized to the corresponding threshold fluence (intensity) of each material.

with the corresponding ΔF values. Most of the data points fall onto the predicted lines; a few exceptions, such as the SiO_2 and CaF_2 data from Ref. [27], are due to inaccuracy in determining ΔF. Nevertheless, the overall agreement demonstrates the prediction power of Eq. (14) for a variety of materials. Particularly, materials with a large bandgap such as FS, CaF_2, sapphire, and soda-lime glass have a high damage threshold F_{th} [35], which makes them a better choice for high-resolution laser lithography, provided that there is flexibility in choosing substrate materials (which is often not the case). In this study, the control resolution in the experimental setup determines ΔF, which in turn determines the smallest feature size $2r_{min}$ that can be produced repeatedly. In addition, it is worth pointing out that there is also a fluctuation of $2r_{min}$ due to laser fluence fluctuation [36] which is not considered in our model.

Optics EXPRESS

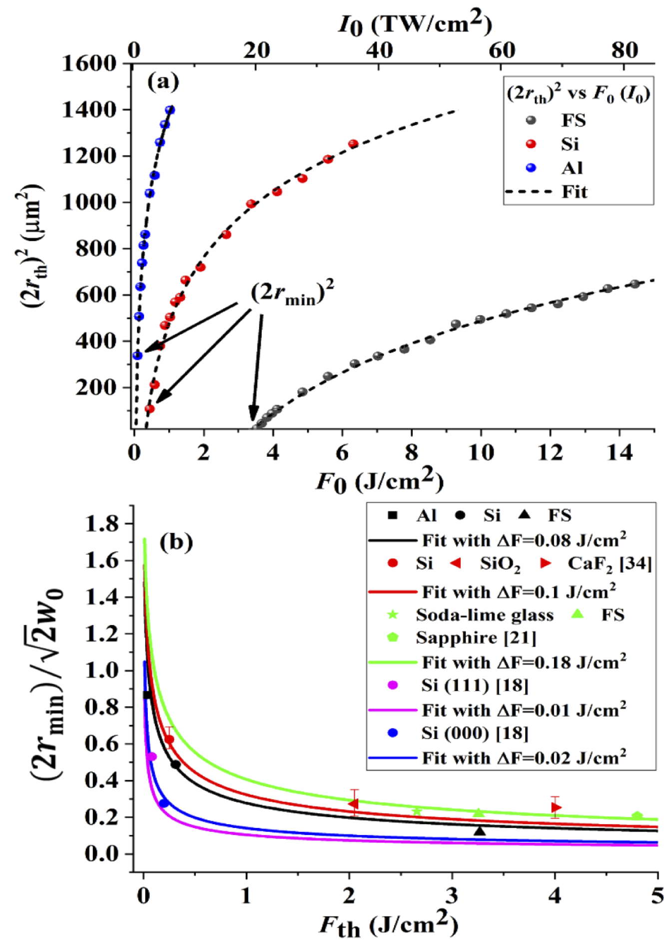

Fig. 3. (a) Square of feature size $(2r_{\text{th}})^2$ as a function of incident laser fluence F_0 and laser intensity I_0 for three materials used in the experiment. This is the same result as in Fig. 2(b) but plotted in the linear scale. (b) Minimum feature size $2r_{\text{min}}$ (nondimensionalized to the laser focal size w_0) that can be achieved in experiments depends on the damage threshold F_{th} of the material used. Data points are from our own results and the literature. The solid lines are fittings based on Eq. (14).

5. Conclusions

To conclude, we have derived a relationship between feature size and laser fluence for band-gap materials, an extension to the well-known formula derived by Liu [18]. We have shown that such a relationship remains the same for single-photon absorption in metals and multiphoton/avalanche absorption in band-gap materials. Single-shot laser lithography experiments on fused silica, silicon, and metal samples have been conducted to verify such invariance, which is later utilized to determine the smallest features that can be fabricated repeatably with different materials. This result can be applied in laser-lithography-based mass production because every laser processing system is subject to a certain level of control resolution, which needs to be taken into consideration in the initial design and the choice of processing parameters.

Funding. National Science Foundation (1846671).

Acknowledgments. The authors thank Dr. Xinpeng Du for his helpful discussion.

Disclosures. The authors declare no conflicts of interest.

References

1. R. R. Gattass and E. Mazur, "Femtosecond laser micromachining in transparent materials," Nat. Photonics **2**(4), 219–225 (2008).
2. D. Du, X. Liu, G. Korn, J. Squier, and G. Mourou, "Laser-induced breakdown by impact ionization in SiO2 with pulse widths from 7 ns to 150 fs," Appl. Phys. Lett. **64**(23), 3071–3073 (1994).
3. P. Pronko, S. Dutta, J. Squier, J. Rudd, D. Du, and G. Mourou, "Machining of sub-micron holes using a femtosecond laser at 800 nm," Opt. Commun. **114**(1-2), 106–110 (1995).
4. B. C. Stuart, M. D. Feit, S. Herman, A. Rubenchik, B. Shore, and M. Perry, "Nanosecond-to-femtosecond laser-induced breakdown in dielectrics," Phys. Rev. B **53**(4), 1749–1761 (1996).
5. B. Stuart, M. Feit, A. Rubenchik, B. Shore, and M. Perry, "Laser-induced damage in dielectrics with nanosecond to subpicosecond pulses," Phys. Rev. Lett. **74**(12), 2248–2251 (1995).
6. B. C. Stuart, M. D. Feit, S. Herman, A. M. Rubenchik, B. W. Shore, and M. D. Perry, "Optical ablation by high-power short-pulse lasers," J. Opt. Soc. Am. B **13**(2), 459–468 (1996).
7. E. G. Gamaly and A. V. Rode, "Physics of ultra-short laser interaction with matter: From phonon excitation to ultimate transformations," Prog. Quantum Electron. **37**(5), 215–323 (2013).
8. M. Li, S. Menon, J. P. Nibarger, and G. N. Gibson, "Ultrafast electron dynamics in femtosecond optical breakdown of dielectrics," Phys. Rev. Lett. **82**(11), 2394–2397 (1999).
9. B. N. Chichkov, C. Momma, S. Nolte, F. Von Alvensleben, and A. Tünnermann, "Femtosecond, picosecond and nanosecond laser ablation of solids," Appl. Phys. A **63**(2), 109–115 (1996).
10. N. Sanner, O. Utéza, B. Chimier, M. Sentis, P. Lassonde, F. Légaré, and J. Kieffer, "Toward determinism in surface damaging of dielectrics using few-cycle laser pulses," Appl. Phys. Lett. **96**(7), 071111 (2010).
11. Y. Liao, W. Pan, Y. Cui, L. Qiao, Y. Bellouard, K. Sugioka, and Y. Cheng, "Formation of in-volume nanogratings with sub-100-nm periods in glass by femtosecond laser irradiation," Opt. Lett. **40**(15), 3623–3626 (2015).
12. R. Wollhofen, J. Katzmann, C. Hrelescu, J. Jacak, and T. A. Klar, "120 nm resolution and 55 nm structure size in STED-lithography," Opt. Express **21**(9), 10831–10840 (2013).
13. B. Zhou, A. Kar, M. Soileau, and X. Yu, "Reducing feature size in femtosecond laser ablation of fused silica by exciton-seeded photoionization," Opt. Lett. **45**(7), 1994–1997 (2020).
14. D. A. Fletcher, K. B. Crozier, K. W. Guarini, S. C. Minne, G. S. Kino, C. F. Quate, and K. E. Goodson, "Microfabricated silicon solid immersion lens," J. Microelectromech. Syst. **10**(3), 450–459 (2001).
15. Q. Li, Q. Wu, Y. Li, C. Zhang, Z. Jia, J. Yao, J. Sun, and J. Xu, "Femtosecond laser-induced periodic surface structures on lithium niobate crystal benefiting from sample heating," Photonics Res. **6**(8), 789–793 (2018).
16. X. Shi, L. Jiang, X. Li, K. Zhang, D. Yu, Y. Yu, and Y. Lu, "Temporal femtosecond pulse shaping dependence of laser-induced periodic surface structures in fused silica," J. Appl. Phys. **116**(3), 033104 (2014).
17. A. P. Joglekar, H.-h. Liu, E. Meyhöfer, G. Mourou, and A. J. Hunt, "Optics at critical intensity: Applications to nanomorphing," Proc. Natl. Acad. Sci. U. S. A. **101**(16), 5856–5861 (2004).
18. J. Liu, "Simple technique for measurements of pulsed Gaussian-beam spot sizes," Opt. Lett. **7**(5), 196–198 (1982).
19. J. Fischer, J. B. Mueller, J. Kaschke, T. J. Wolf, A.-N. Unterreiner, and M. Wegener, "Three-dimensional multi-photon direct laser writing with variable repetition rate," Opt. Express **21**(22), 26244–26260 (2013).
20. M. Gedvilas, J. Mikšys, J. Berzinš, V. Stankevič, and G. Račiukaitis, "Multi-photon absorption enhancement by dual-wavelength double-pulse laser irradiation for efficient dicing of sapphire wafers," Sci. Rep. **7**(1), 5218 (2017).
21. M. Garcia-Lechuga, O. Utéza, N. Sanner, and D. Grojo, "Evidencing the nonlinearity independence of resolution in femtosecond laser ablation," Opt. Lett. **45**(4), 952–955 (2020).
22. J. Bonse, S. Baudach, J. Krüger, W. Kautek, and M. Lenzner, "Femtosecond laser ablation of silicon–modification thresholds and morphology," Appl. Phys. A **74**(1), 19–25 (2002).

Optics EXPRESS

23. J. Jandeleit, G. Urbasch, H. Hoffmann, H.-G. Treusch, and E. Kreutz, "Picosecond laser ablation of thin copper films," Appl. Phys. A **63**(2), 117–121 (1996).
24. J. Byskov-Nielsen, J.-M. Savolainen, M. S. Christensen, and P. Balling, "Ultra-short pulse laser ablation of metals: threshold fluence, incubation coefficient and ablation rates," Appl. Phys. A **101**(1), 97–101 (2010).
25. S.-S. Wellershoff, J. Hohlfeld, J. Güdde, and E. Matthias, "The role of electron–phonon coupling in femtosecond laser damage of metals," Appl. Phys. A **69**(S1), S99–S107 (1999).
26. P. Zhokhov and A. Zheltikov, "Optical breakdown of solids by few-cycle laser pulses," Sci. Rep. **8**(1), 1824 (2018).
27. A. Mouskeftaras, M. Chanal, M. Chambonneau, R. Clady, O. Utéza, and D. Grojo, "Direct measurement of ambipolar diffusion in bulk silicon by ultrafast infrared imaging of laser-induced microplasmas," Appl. Phys. Lett. **108**(4), 041107 (2016).
28. E. J. Yoffa, "Dynamics of dense laser-induced plasmas," Phys. Rev. B **21**(6), 2415–2425 (1980).
29. A. Rahaman, A. Kar, and X. Yu, "Thermal effects of ultrafast laser interaction with polypropylene," Opt. Express **27**(4), 5764–5783 (2019).
30. L. Nguyen, T. Hashimoto, D. N. Zakharov, E. A. Stach, A. P. Rooney, B. Berkels, G. E. Thompson, S. J. Haigh, and T. L. Burnett, "Atomic-scale insights into the oxidation of aluminum," ACS Appl. Mater. Interfaces **10**(3), 2230–2235 (2018).
31. T. Campbell, R. K. Kalia, A. Nakano, P. Vashishta, S. Ogata, and S. Rodgers, "Dynamics of oxidation of aluminum nanoclusters using variable charge molecular-dynamics simulations on parallel computers," Phys. Rev. Lett. **82**(24), 4866–4869 (1999).
32. A. Žemaitis, M. Gaidys, P. Gečys, and M. Gedvilas, "Influence of nonlinear and saturable absorption on laser lift-off threshold of an oxide/metal structure," Opt. Lett. **45**(22), 6166–6169 (2020).
33. A. Žemaitis, M. Gaidys, M. Brikas, P. Gečys, G. Račiukaitis, and M. Gedvilas, "Advanced laser scanning for highly-efficient ablation and ultrafast surface structuring: experiment and model," Sci. Rep. **8**(1), 1–14 (2018).
34. F. Korte, J. Serbin, J. Koch, A. Egbert, C. Fallnich, A. Ostendorf, and B. Chichkov, "Towards nanostructuring with femtosecond laser pulses," Appl. Phys. A **77**(2), 229–235 (2003).
35. L. Gallais, D.-B. Douti, M. Commandre, G. Batavičiūtė, E. Pupka, M. Ščiuka, L. Smalakys, V. Sirutkaitis, and A. Melninkaitis, "Wavelength dependence of femtosecond laser-induced damage threshold of optical materials," J. Appl. Phys. **117**(22), 223103 (2015).
36. M. Garcia-Lechuga, G. G. El Reaidy, H. Ning, P. Delaporte, and D. Grojo, "Assessing the limits of determinism and precision in ultrafast laser ablation," Appl. Phys. Lett. **117**(17), 171604 (2020).

132.170.15.255 {ts '2021-02-05 11:27:24'}